Research Article Vol. 35, No. 1 / January 2018 / Journal of the Optical Society of America A 65

Journal of the Optical Society of America A

OPTICS, IMAGE SCIENCE, AND VISION

Trajectories on the Poincaré sphere of polarization states of a beam passing through a rotating linear retarder

KAROL SALAZAR-ARIZA AND RAFAEL TORRES*

Grupo de Óptica y Tratamiento de Señales, Universidad Industrial de Santander, Bucaramanga, Colombia
**Corresponding author: rafael.torres@saber.uis.edu.co*

Received 14 September 2017; revised 8 November 2017; accepted 13 November 2017; posted 13 November 2017 (Doc. ID 307082); published 12 December 2017

The emerging polarization states from a linearly polarized monochromatic light passing through a rotating linear quarter-wave plate have been characterized as the intersection curve of a cylinder and the Poincaré sphere. But in the cases where the input polarization states are in general elliptical or circular and pass through a rotating linear retarder, the emerging polarization states produce trajectories that do not correspond to the intersection of a sphere with one cylinder. Hence, in this work, we present a full characterization of the trajectories on the Poincaré sphere for monochromatic input beams with an arbitrary polarization state passing through a rotating linear retarder as the intersection curve of the Poincaré sphere with a cone. Moreover, it is shown that these trajectories are characterized by their projection on the equator plane, having the form of *limaçon* of Pascal (Pascal's snails).

OCIS codes: (260.5430) Polarization; (260.1440) Birefringence; (260.2130) Ellipsometry and polarimetry.

https://doi.org/10.1364/JOSAA.35.000065

1. INTRODUCTION

Birefringent retarder plates allow transformation of a polarization state into another in a controlled manner [1–5], becoming an important component for the development of applications in different areas such as in polarimetry [6,7], in medicine and biology for the characterization of cells and tissues [8–12], in industrial processes [13,14], and in the study of optical properties of materials [15–19], among others.

It has been shown that polarized monochromatic beams passing through a quarter-wave rotating retarder describe interesting paths on the Poincaré sphere [20]. One of these paths corresponds to the intersection of the Poincaré sphere with a cylinder in the case of linearly polarized beams that pass through a quarter-wave rotating retarder [21]. The characterization of these paths is useful because it allows us to know in advance all emerging polarization states for a polarized monochromatic beam passing through a rotating linear retarder. Nevertheless, beams with elliptical polarization states passing through a rotating linear retarder result in polarization states describing trajectories on the Poincaré sphere not corresponding to the intersection curve between the Poincaré sphere and a cylinder.

The retarder is important in the optimization of polarimeters based on rotating retarders, as shown in the works of Ambirajan and Look [22,23], where they use a quarter-wave rotating retarder and a fixed linear polarizer. On the other hand, Sabatke *et al.* show that a retarder with retardance of 132° provides an improvement in signal-to-noise ratio [24,25]. Hence, in this work we formulate a full characterization of all states of polarization of output beams passing through the rotating linear retarder as the curve of intersection of a cone with the Poincaré sphere. For this purpose, we use the Stokes–Mueller formulation for polarized light, which allows us to describe arbitrary optical elements [26,27].

This paper is organized as follows: In Section 2 are described the trajectories on the Poincaré sphere representing all output of polarization states that a polarized beam passing through a rotating linear retarder can have. In Section 3 we obtain the intersection curve of the Poincaré sphere with a cone and its geometric interpretation. Sections 4 and 5 illustrate the results of Sections 2 and 3 for the cases: quarter-wave rotating retarder and half-wave rotating retarder. Finally, in Section 6, the results obtained in Sections 2 and 3 are checked experimentally for the case of a quarter-wave rotating retarder.

2. FORMULATION OF THE PATHS ON THE POINCARÉ SPHERE

To determine the trajectories that describe the emerging polarization states of a monochromatic polarized beam passing

through a rotating linear retarder, we used the general Mueller matrix.

For a general linear retarder with δ, the phase difference between the fast and slow axis and θ is the angle of the fast axis of the retarder with respect to the horizontal; the emergent polarization state is obtained by multiplying the corresponding Mueller matrix by the state of the polarized input beam, resulting in Eq. (1), where the angles 2χ and 2α are the coordinates of the input state on the Poincaré sphere

$$\begin{pmatrix} S_0' \\ S_1' \\ S_2' \\ S_3' \end{pmatrix} = \begin{pmatrix} 1 \\ \cos 2\chi \cos 2\alpha + [\cos 2\chi \sin(2\alpha - 2\theta)(1 - \cos\delta) + \sin 2\chi \sin\delta]\sin 2\theta \\ \cos 2\chi \sin 2\alpha - [\cos 2\chi \sin(2\alpha - 2\theta)(1 - \cos\delta) + \sin 2\chi \sin\delta]\cos 2\theta \\ \sin\delta \cos 2\chi \sin(2\alpha - 2\theta) + \sin 2\chi \cos\delta \end{pmatrix}. \tag{1}$$

So, depending on the input polarization state, which propagates through the rotating linear birefringent plate that rotates from 0° to 180°, the emerging state $\mathbf{S}' = (S_0', S_1', S_2', S_3')$, Eq. (1), forms interesting trajectories on the Poincaré sphere. These trajectories, as will be shown in the following section, are characterized by the intersection of the Poincaré sphere with a cone.

3. GEOMETRIC INTERPRETATION: INTERSECTION OF A SPHERE AND A CONE

Azzam, in [21], shows that the trajectory corresponding to a linearly polarized state passing through a rotating quarter-wave linear retarder is characterized by the intersection between the sphere of Poincaré and a cylinder. Nevertheless, the intersection curves between a sphere with a cone, called the Monge cone (see [28,29]), are of greater interest for our study, because, as will be shown later, it can also characterize all curves that occur when a polarized beam passes through a rotating linear retarder.

Theorem 1. *The locus of all points formed by the emerging polarization states of a rotating birefringent linear wave plate from an input polarized beam corresponds to the intersection of the Poincaré sphere with a cone.*

Proof 1. *The equation of a sphere centered at the origin is*

$$x^2 + y^2 + z^2 = 1, \tag{2}$$

and the equation of a cone oriented around an axis parallel to the z axis, with vertex at (a, b, c) is written

$$(x - a)^2 + (y - b)^2 = \tan^2\left(\frac{\delta}{2}\right)(z - c)^2, \tag{3}$$

where δ is the angle of the cone. Using tangent half-angle formula, we obtain

$$(x - a)^2 + (y - b)^2 = \left(\frac{1 - \cos\delta}{\sin\delta}\right)^2 (z - c)^2. \tag{4}$$

We take $a^2 + b^2 + c^2 = 1$, i.e., the vertex is on the Poincaré sphere. Then, the interception is obtained from the parameterization of variables x and y, defined by equations

$$x = a + \left(\frac{1 - \cos\delta}{\sin\delta}\right)(z - c)\sin 2t, \tag{5}$$

and

$$y = b - \left(\frac{1 - \cos\delta}{\sin\delta}\right)(z - c)\cos 2t. \tag{6}$$

Substituting the above equations in Eq. (2), we obtain

$$\begin{aligned} &c^2\left[\left(\frac{1 - \cos\delta}{\sin\delta}\right)^2 - 1\right] + 2c\left(\frac{1 - \cos\delta}{\sin\delta}\right)(b\cos 2t - a\sin 2t) \\ &- 2z\left(\frac{1 - \cos\delta}{\sin\delta}\right)\left[b\cos 2t - a\sin 2t + c\left(\frac{1 - \cos\delta}{\sin\delta}\right)\right] \\ &+ z^2\left[1 + \left(\frac{1 - \cos\delta}{\sin\delta}\right)^2\right] = 0, \end{aligned} \tag{7}$$

a quadratic algebraic equation for variable z. Defining

$$C = c^2\left[\left(\frac{1 - \cos\delta}{\sin\delta}\right)^2 - 1\right] + 2c\left(\frac{1 - \cos\delta}{\sin\delta}\right)(b\cos 2t - a\sin 2t), \tag{8}$$

$$B = -2\left(\frac{1 - \cos\delta}{\sin\delta}\right)\left[b\cos 2t - a\sin 2t + c\left(\frac{1 - \cos\delta}{\sin\delta}\right)\right], \tag{9}$$

and

$$A = \left[1 + \left(\frac{1 - \cos\delta}{\sin\delta}\right)^2\right]. \tag{10}$$

Its solutions are

$$z_{\pm} = \frac{-B \pm \sqrt{B^2 - 4AC}}{2A}. \tag{11}$$

The vertex of the cone is represented by a point on the Poincaré sphere with coordinates

$$\langle a, b, c\rangle = \langle \cos 2\alpha' \cos 2\chi', \sin 2\alpha' \cos 2\chi', \sin 2\chi'\rangle, \tag{12}$$

where $0 \le \alpha < \pi$ and $-\pi/4 \le \chi \le \pi/4$.

Substituting the coordinates of the vertex in Eq. (11), we obtain for the radical

$$\begin{aligned} &B^2 - 4AC \\ &= \frac{1}{2\left(1 + \left(\frac{1-\cos\delta}{\sin\delta}\right)^2\right)}\left(4\left(\frac{1 - \cos\delta}{\sin\delta}\right)^2 \cos^2 2\chi' \sin^2(2\alpha' - 2t)\right. \\ &\left. -8\sin(2\alpha' - 2t)\sin 2\chi' \cos 2\chi'\left(\frac{1 - \cos\delta}{\sin\delta}\right) + 4\sin^2 2\chi'\right) \\ &= 4\left[\left(\frac{1 - \cos\delta}{\sin\delta}\right)\cos 2\chi' \sin(2\alpha' - 2t) - \sin 2\chi'\right]^2. \end{aligned} \tag{13}$$

Replacing the previous equation in Eq. (11), we obtain

$$z_{\pm} = \frac{2\left(\frac{1-\cos\delta}{\sin\delta}\right)\left[\cos 2\chi' \sin(2\alpha' - 2t) + \sin 2\chi'\left(\frac{1-\cos\delta}{\sin\delta}\right)\right]}{2\left(1 + \left(\frac{1-\cos\delta}{\sin\delta}\right)^2\right)} \pm \frac{2\left[\left(\frac{1-\cos\delta}{\sin\delta}\right)\cos 2\chi' \sin(2\alpha' - 2t) - \sin 2\chi'\right]}{2\left(1 + \left(\frac{1-\cos\delta}{\sin\delta}\right)^2\right)}, \quad (14)$$

where one solution is

$$z_{+} = \sin\delta \cos 2\chi' \sin(2\alpha' - 2t) - \sin 2\chi' \cos\delta, \quad (15)$$

with $0 \le 2t \le \pi$. *Replacing the above solution in Eqs. (5) and (6), we obtain the following equations:*

$$x_{+} = \cos 2\chi' \cos 2\alpha' + [\cos 2\chi' \sin(2\alpha' - 2\theta)(1 - \cos\delta) - \sin 2\chi' \sin\delta]\sin 2\theta, \quad (16)$$

and

$$y_{+} = \cos 2\chi' \sin 2\alpha' - [\cos 2\chi' \sin(2\alpha' - 2\theta)(1 - \cos\delta) - \sin 2\chi' \sin\delta]\cos 2\theta. \quad (17)$$

The last three equations constitute the parametric equations with $0 \le t \le \pi$ *obtained from the intersection curve of the Poincaré sphere and a cone. So this corresponds to the Stokes parameters* (S_1, S_2, S_3) *of Eq. (1) when* $2\alpha' = 2\alpha$ *and* $2\chi' = -2\chi$. *Q.E.D.*

This demonstrates that the cone vertex is in the state $\mathbf{S}(2\alpha, -2\chi)$, which has the same ellipticity and orientation of the input state but rotated in the opposite direction, so we coined the term *enantiogyre* states (from ancient Greek *ἐναντίος*, *enantíos*–opposite–and *γῦρος*, *gyrus*–turning–) by means of the following definition:

Definition 1 (Enantiogyre polarization states). *Two polarization states are defined as enantiogyres if they have the same orientation and ellipticity, but rotate in opposite directions. So, for a polarization state* $\mathbf{S}(2\alpha, 2\chi)$ *its enantiogyre state is defined by* $\mathbf{S}'(2\alpha, -2\chi)$. *In Fig. 1 the states p and p′ are enantiogyres.*

In practice, the most commonly used retarders are $\delta = \pi/2$ and $\delta = \pi$, so we will use them to illustrate the above results.

4. QUARTER-WAVE ROTATING RETARDER

To determine the trajectories that describe the emerging polarization states of a monochromatic polarized beam passing through a rotating linear birefringent quarter-wave plate, the out state (QWP) is written as

$$\mathbf{S}' = \begin{pmatrix} 1 \\ (\cos 2\chi \cos 2\alpha + [\cos 2\chi \sin(2\alpha - 2\theta) + \sin 2\chi]\sin 2\theta) \\ (\cos 2\chi \sin 2\alpha - [\cos 2\chi \sin(2\alpha - 2\theta) + \sin 2\chi]\cos 2\theta) \\ \cos 2\chi \sin(2\alpha - 2\theta) \end{pmatrix}. \quad (18)$$

The emerging state $\mathbf{S}'$ forms interesting trajectories on the Poincaré sphere. Among these trajectories are five cases that deserve special study.

A. Case 1. Locus for Input Linear Polarization State with $\chi = 0$

If input beam $\mathbf{S}(2\alpha, 0)$ is linearly polarized, the emerging polarization states are determined by

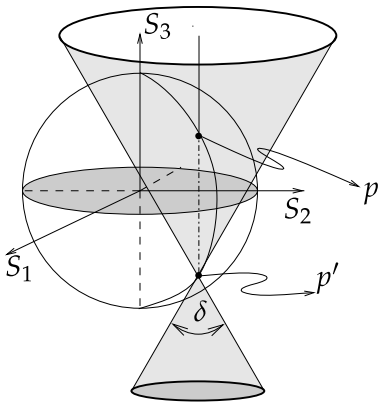

Fig. 1. Trajectories on the Poincaré sphere are characterized by the curve of intersection of the Poincaré sphere with a cone, where the axis of symmetry is defined by the points representing the polarization state of input beam p and its enantiogyre states p', the state associated with the vertex of the cone.

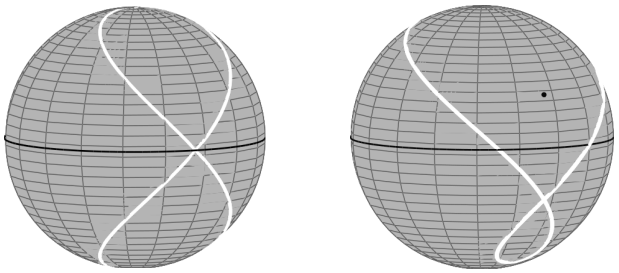

(a) Case 1 (b) Case 1

Fig. 2. Computational simulation of Eq. (18). Locus of the emerging polarization states (a) from a linearly polarized input beam; (b) with asymmetrical eight-shape.

$$\mathbf{S}'(2\alpha, 0) = \begin{pmatrix} 1 \\ \cos(2\alpha - 2\theta)\cos 2\theta \\ \cos(2\alpha - 2\theta)\sin 2\theta \\ \sin(2\alpha - 2\theta) \end{pmatrix}. \quad (19)$$

The vectorial part corresponds to Viviani's curve [30,31], which can be obtained from the intersection of a cylinder with the Poincaré sphere, as Azzam evidences in his paper [21].

Graphing Eq. (19) for $0 \le \theta \le \pi$ results in a symmetrical eight-shape, as shown in Fig. 2(a), where the point of intersection corresponds to the linear polarization state of the input beam, indicating that it is an eigenstate of the linear birefringent retarder. For $2\alpha - 2\theta = \pm\pi/2$, the output states are circulars, right or left, respectively.

B. Case 2. Locus for Input State with $0 < |2\chi| < \pi/4$

The emerging polarization states, determined by Eq. (18), describe asymmetrical eight-shape trajectories, as shown in Fig. 2(b).

We are going to study this case in detail, which we could call the general case, in order to be able to understand the characteristics of these trajectories.

1. Emerging States at the Same Meridian as Input Beam State

In the asymmetric eight-shape curve [Fig. 2(b)], some states are on the same meridian as the input beam state $\mathbf{S}_{\text{input}}(2\alpha, 2\chi)$, i.e., $2\alpha' = 2\alpha$ or $2\alpha' = 2\alpha + \pi \bmod(2\pi)$; we define these states as $\mathbf{S}_{\text{upper}}(2\alpha', 2\chi')$, $\mathbf{S}_{\text{cross}}(2\alpha', 2\chi')$, and $\mathbf{S}_{\text{lower}}(2\alpha', 2\chi')$ (see Fig. 3).

To find these polarization states, we first calculate the angle θ using Eq. (18), which keeps the meridian invariant. Since $\cos(2\alpha + \pi) = -\cos 2\alpha$ and $\sin(2\alpha + \pi) = -\sin 2\alpha$, we have

$$\pm \cos 2\chi' \cos 2\alpha = \cos 2\chi \cos 2\alpha + [\cos 2\chi \sin(2\alpha - 2\theta) + \sin 2\chi] \sin 2\theta, \tag{20}$$

$$\pm \cos 2\chi' \sin 2\alpha = \cos 2\chi \sin 2\alpha - [\cos 2\chi \sin(2\alpha - 2\theta) + \sin 2\chi] \cos 2\theta, \tag{21}$$

and

$$\sin 2\chi' = \cos 2\chi \sin(2\alpha - 2\theta). \tag{22}$$

Solving Eqs. (20) and (21) for $\cos 2\chi'$ and equaling them, we have

$$[\cos 2\chi \sin(2\alpha - 2\theta) + \sin 2\chi] \cos(2\theta - 2\alpha) = 0. \tag{23}$$

So, for θ we obtain the following four solutions:

$$2\theta_1 = 2\alpha - \arcsin(-\tan 2\chi), \tag{24}$$

$$2\theta_2 = 2\alpha + \arcsin(-\tan 2\chi) - \pi, \tag{25}$$

$$2\theta_- = 2\alpha - \pi/2, \tag{26}$$

$$2\theta_+ = 2\alpha + \pi/2, \tag{27}$$

which determine the four points of the path that cross the meridian corresponding to the polarization state of the input beam.

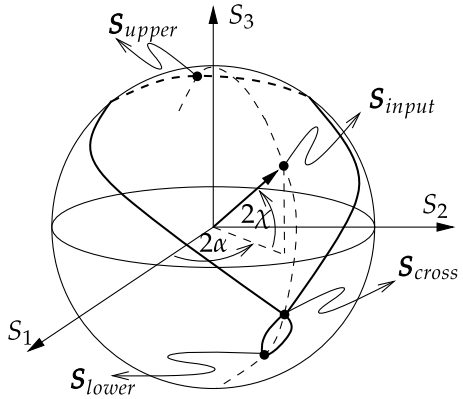

Fig. 3. Scheme of asymmetrical eight-curve, for an input state $\mathbf{S}_{\text{input}}$; the output states at the same meridian are $\mathbf{S}_{\text{upper}}$, $\mathbf{S}_{\text{cross}}$, and $\mathbf{S}_{\text{lower}}$.

2. Intersection State

By replacing θ_1 and θ_2 in Eq. (18) (see Appendix A) we obtain the same emerging polarization state resulting in

$$\mathbf{S}'_{\text{cross}}(2\alpha, 2\chi) = \begin{pmatrix} 1 \\ \cos 2\chi \cos 2\alpha \\ \cos 2\chi \sin 2\alpha \\ -\sin 2\chi \end{pmatrix}, \tag{28}$$

and this corresponds to the intersection point of the trajectory on the Poincaré sphere. Therefore, if the input state is $\mathbf{S}_{\text{input}} = \mathbf{S}(2\alpha, 2\chi)$, then the intersection state is $\mathbf{S}_{\text{cross}} = \mathbf{S}(2\alpha, -2\chi)$, which means that the state at the point of intersection and the input beam state are enantiogyre polarization states (see Fig. 1).

3. Upper and Lower States

From the other two solutions θ_- and θ_+, replacing in Eq. (18) (see Appendix B), result in the minimum and maximum value of parameter $2\chi'$ for the emerging polarization state. Because of the symmetry in the Poincaré sphere, we are going to discuss here only the case of an input polarization state in the northern hemisphere, i.e., $\chi > 0$.

The emerging polarization state with the minimum value of $2\chi'$, i.e., for θ_-, is

$$\mathbf{S}_{\text{lower}}(2\alpha', 2\chi') = \begin{pmatrix} 1 \\ \sin 2\chi \cos 2\alpha \\ \sin 2\chi \sin 2\alpha \\ -\cos 2\chi \end{pmatrix}, \tag{29}$$

where it is noted that $2\chi' = 2\chi - \pi/2$ and $\alpha' = \alpha$. The emerging polarization state with maximum value of $2\chi'$, i.e., for θ_+, is

$$\mathbf{S}_{\text{upper}}(2\alpha', 2\chi') = \begin{pmatrix} 1 \\ -\sin 2\chi \cos 2\alpha \\ -\sin 2\chi \sin 2\alpha \\ \cos 2\chi \end{pmatrix}; \tag{30}$$

then, $2\chi' = \pi/2 - 2\chi$ and $2\alpha' = 2\alpha + \pi$. So, we write

$$\mathbf{S}_{\text{upper}} = \mathbf{S}(2\alpha + \pi, \pi/2 - 2\chi), \tag{31}$$

and the lowest point is given by

$$\mathbf{S}_{\text{lower}} = \mathbf{S}(2\alpha, 2\chi - \pi/2), \tag{32}$$

which means that $\mathbf{S}_{\text{upper}}$ and $\mathbf{S}_{\text{lower}}$ are diametrically opposite; therefore they are orthogonal polarization states (see Fig. 4).

Then, the ellipticity of the output beam is limited by $|2\chi'| \leq \pi/2 - |2\chi|$, where χ is the ellipticity of the input beam.

Remark 1. *The polarization states on the Poincaré sphere that are below the lowest point, or above the highest point, are states which cannot be accessed by combining retarders QWP and a half-wave plate from an arbitrary elliptical input state.*

C. Case 3. Input Polarization State with Ellipticity $2\chi = \pm\pi/4$

In the case where the input beam has a polarization state with ellipticity $2\chi = \pm\pi/4$, we obtained the emerging polarization states path

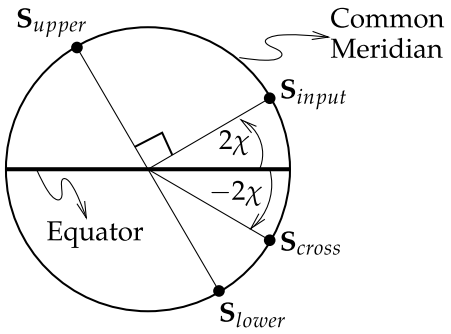

Fig. 4. Scheme of the plane of the meridian where the states $\mathbf{S}_{\text{input}}$, $\mathbf{S}_{\text{upper}}$, $\mathbf{S}_{\text{lower}}$, and $\mathbf{S}_{\text{cross}}$ are located. The states $\mathbf{S}_{\text{upper}}$ and $\mathbf{S}_{\text{lower}}$ are diametrically opposed.

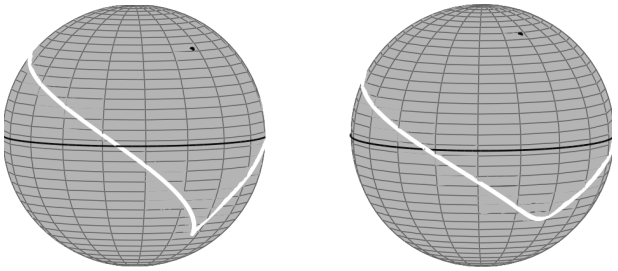

(a) Case 3 (b) Case 4

Fig. 5. Emerging states for (a) input polarized beam with ellipticity $2\chi = \pi/4$; (b) input polarized beam with ellipticity $\pi/4 < 2\chi < \pi/2$.

$$\mathbf{S}' = \begin{pmatrix} 1 \\ \frac{1}{\sqrt{2}}[\cos 2\alpha + (\sin(2\alpha - 2\theta) + 1)\sin 2\theta] \\ \frac{1}{\sqrt{2}}[\sin 2\alpha - (\sin(2\alpha - 2\theta) + 1)\cos 2\theta] \\ \frac{1}{\sqrt{2}}\sin(2\alpha - 2\theta) \end{pmatrix}. \quad (33)$$

This equation describes a trajectory that is not an asymmetrical eight-shape on the Poincaré sphere, as shown in Fig. 5(a).

D. Case 4. Input Polarization State with Ellipticity $\pi/4 < |2\chi| < \pi/2$

When the polarization state of the input beam has ellipticity $\pi/4 < 2\chi < \pi/2$, the emerging states are obtained by Eq. (18), which describes a trajectory on the Poincaré sphere without intersection, as shown in Fig. 5(b).

In these cases, the enantiogyre state of the input beam state is not one state of polarization of the emerging beam, i.e., it is not a point of the trajectory on the Poincaré sphere, because Eqs. (24) and (25) no longer have a solution.

E. Case 5. Input Circular Polarization State $|2\chi| = \pi/2$

When the input beam is circularly polarized and passes through a rotating retarder, emerging polarization states are determined by

$$\mathbf{S}' = \begin{pmatrix} 1 \\ \sin 2\theta \\ -\cos 2\theta \\ 0 \end{pmatrix}, \quad (34)$$

forming a distribution of points on the equator of the Poincaré sphere, i.e., all output polarization states are linearly polarized.

F. Projection on the (S_1, S_2) Coordinate Plane

A characterization of the different curves is to take its projections on the equator plane (S_1, S_2) (see Fig. 6), which are the *limaçon* of Pascal (Pascal's snails) [32,33].

Proposition 1. *The projection on the equator plane of the trajectories of emerging polarization states of a QWP from an input polarized light beam corresponds to limaçon of Pascal, oriented according to the input polarization state.*

Proof 2. *Beginning from Eq. (18), the general equation of the trajectories on the Poincaré sphere, the projections on the* (S_1, S_2) *plane correspond to taking component* S_3 *equal to zero; then*

$$\begin{aligned}(S_1, S_2) = (1, &\cos 2\chi \cos 2\alpha + \cos 2\chi \sin 2\alpha \cos 2\theta \sin 2\theta \\ &- \cos 2\chi \cos 2\alpha \sin^2 2\theta + \sin 2\chi \sin 2\theta, \\ &\cos 2\chi \sin 2\alpha + \cos 2\chi \sin 2\alpha \cos^2 2\theta \\ &- \cos 2\chi \cos 2\alpha \sin 2\theta \cos 2\theta + \sin 2\chi \cos 2\theta). \end{aligned} \quad (35)$$

We define $a = \cos 2\chi \cos 2\alpha$, $b = \cos 2\chi \sin 2\alpha$ *and* $c = \sin 2\chi$, *thus*

$$\begin{aligned}(S_1, S_2) = (1, &a + b \cos 2\theta \sin 2\theta - a \sin^2 2\theta + c \sin 2\theta, \\ &b - b \cos^2 2\theta + a \sin 2\theta \cos 2\theta - c \cos 2\theta), \end{aligned} \quad (36)$$

simplifying

$$\begin{aligned}(S_1, S_2) = \left(1, a + \frac{b \sin 4\theta}{2} - a\left(\frac{1 - \cos 4\theta}{2}\right) + c \sin 2\theta, \right. \\ \left. b - b\left(\frac{1 + \cos 4\theta}{2}\right) + \frac{a \sin 4\theta}{2} - c \cos 2\theta\right), \end{aligned} \quad (37)$$

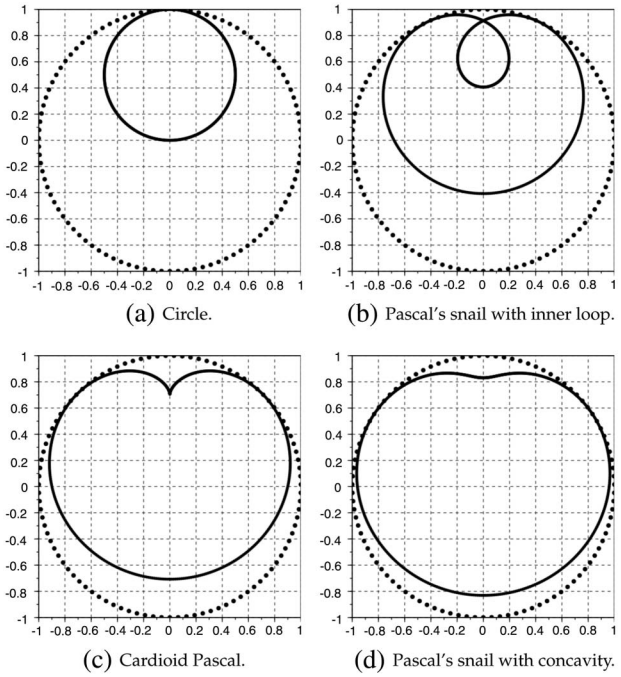

(a) Circle. (b) Pascal's snail with inner loop.

(c) Cardioid Pascal. (d) Pascal's snail with concavity.

Fig. 6. Projections on the plane (e_1, e_2) corresponding to the curves. (a) Projection of Fig. 2(a); (b) projection of Fig. 2(b); (c) projection of Fig. 5(a); (d) projection of Fig. 5(b).

Finally, we have

$$S_1 = \frac{a}{2} + \frac{b \sin 4\theta}{2} + \frac{a \cos 4\theta}{2} + c \sin 2\theta, \quad (38)$$

$$S_2 = \frac{b}{2} - \frac{b \cos 4\theta}{2} + \frac{a \sin 4\theta}{2} - c \cos 2\theta, \quad (39)$$

which are generalized parametric equations of limaçon of Pascal, where 2α determines the orientation of the limaçon and 2χ characterizes the different curves that arise as special cases.

Figure 6(a) shows the projections of the symmetrical eight-shape curve [Fig. 2(a)], Viviani's curve. From here, we can see that this path can be interpreted as the intersection of a sphere and one cylinder whose diameter is 1.

The projections in Figs. 6(b)–6(d), correspond to the *limaçon* of Pascal, taking $\alpha = \pi/4$. In Fig. 6(b) the *limaçon* is a triseptrix; in Fig. 6(c) the *limaçon* degenerates in a cardioid, and in Fig. 6(d) the *limaçon* is concave. As the input beam state approaches the pole, the *limaçon* becomes convex.

Remark 2. *It can be noted in Figs. 2(b), 5(a), and 5(b) and their projections in Fig. 6, that these paths cannot be adapted by the intersection of a sphere and a cylinder.*

5. HALF-WAVE ROTATING RETARDER

In the event that a polarized beam passes through a half-wave rotating retarder, the equation of a cone [see Eq. (4)] degenerates in the equation of a plane $z = -\sin 2\chi$. The intersection curve between the plane and Poincaré sphere is a circle (see Fig. 7), which corresponds to the parallel where the enantiogyre state of the input state is.

6. SIMULATION AND EXPERIMENT OF A ROTATING QWP

The setup used in the laboratory represented in Fig. 8 allows us to generate the different trajectories that describe the output polarization states from an input polarized monochromatic beam passing through a linear birefringent QWP that is rotated from 0° to 180°. The experimental measures are done using a commercial Thorlabs polarimeter (*PAN*5710*VIS*, S/N: *M*00255491). The input beam is prepared from a nonpolarized He–Ne laser (632.8 nm), which is polarized passing through a linear polarizer (P), a quarter-wave plate (Q), and then by a half-wave plate (H).

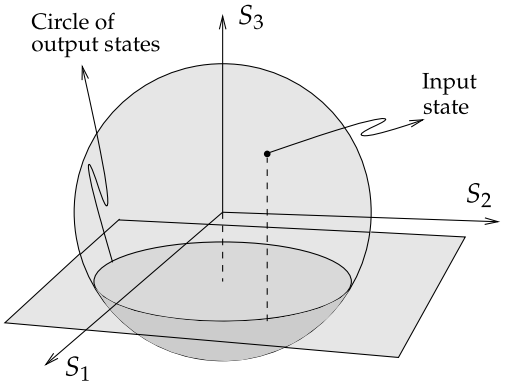

Fig. 7. Emerging states from a half-wave plate rotating.

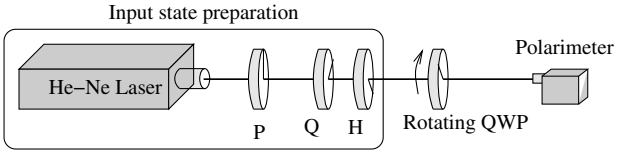

Fig. 8. Schematization of the optical system for the recording of experimental data.

The trajectories on the Poincaré sphere obtained experimentally fit very well with the curve expressed in Eq. (18), as will be shown below. In all cases, the cone has its vertex in the enantiogyre state of the input beam polarization state. The cone axis is determined by the straight line defined by the points of the input beam polarization state p and its enantiogyre state p' (the cone vertex); see Fig. 1.

In Fig. 9 are superimposed the simulated data using Eq. (18), red dots, the curve resulting from the intersection of the Poincaré sphere with the cone and the data taken in the experimental setup; blue dots and the white dot correspond to the input beam state.

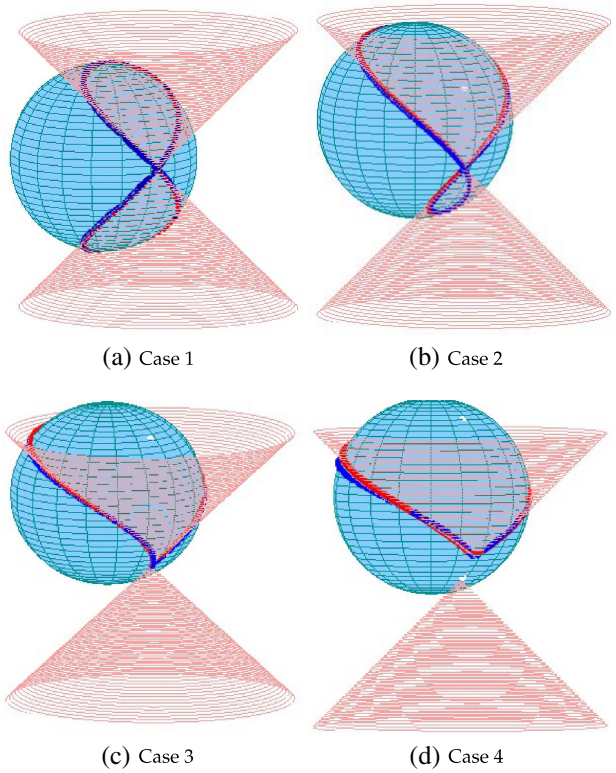

Fig. 9. Red paths correspond to the data calculated from Eq. (18), and the blue paths correspond to the experimental data. The trajectories are characterized by the curve of intersection of the Poincaré sphere and a cone. (a) Case 1, input linear polarization state $\mathbf{S}(\pi/2, 0)$; (b) Case 2, input polarization state $\mathbf{S}(\pi/2, 0.1311\pi)$; (c) Case 3; input polarization state $\mathbf{S}(\pi/2, \pi/4)$; (d) Case 4, input polarization state $\mathbf{S}(\pi/2, 0.3120\pi)$.

Remark 3. *The vertex of the cone on the Poincaré sphere corresponding to the intersection point [see Eq. (28)] is related to the polarization state of the input beam by the following equation:*

$$V(2\alpha, \mp 2\chi) = \mathbf{S}(2\alpha, \pm 2\chi), \tag{40}$$

which characterizes fully the intersection curve describing the emerging polarization states that a beam can have after passing through the rotating quarter-wave retarder.

A. Analysis of Results

An input beam state with ellipticity $\chi = 0$ (linearly polarized), which corresponds to a point on the equator of the Poincaré sphere, has the shape known as Viviani's curve; see Fig. 9(a). Furthermore, the linear polarization input state is an eigenstate of linear birefringent and corresponds to the vertex of the cone.

For an input beam state with ellipticity $0 < |2\chi| < \pi/4$ [Fig. 9(b)], the path takes the form of an asymmetrical eight, where the vertex of the cone is located in the polarization state corresponding to the curve intersection point, which is the enantiogyre state of the input state.

When the input beam has a polarization state $\mathbf{S}(\pi/2, \pi/4)$, the vertex of the cone is in $V(\pi/2, -\pi/4)$, and the curve has no intersection, because only the top part of the cone linked to the vertex intersects the Poincaré sphere, as shown in Fig. 9(c), considered as a limiting case in Section 4. In this case, the bottom part of the cone and the sphere are tangent; therefore, the intersection only occurs with the vertex.

For an input beam state with ellipticity $\pi/4 < |2\chi| < \pi/2$, the vertex of the cone is no longer part of the path describing the state's emerging polarization [Fig. 9(d)]. Furthermore, as the polarization state of the input beam approaches the north pole of the Poincaré sphere, the vertex of the cone approaches the south pole, so that the intersection curve becomes the equator.

Finally, an input beam state with ellipticity $|2\chi| = \pm\pi/2$ (circular polarization), the vertex is on the south pole (north pole) of the Poincaré sphere, and the intersection corresponds to the equator [Eq. (34)], describing all linear polarization emerging states.

7. CONCLUSIONS

We summarize the results here found by means of the following law:

Law 1. *The trajectories formed on the Poincaré sphere as a result of passing a polarized beam through a rotating linear retarder are characterized by the intersection curves of the Poincaré sphere and a cone. The axis of symmetry of the cone is defined by the polarization state of the input beam and its enantiogyre state, where the vertex of the cone is (see Fig. 1). The projections on the plane of the equator of these curves corresponds to the limaçon of Pascal.*

APPENDIX A: PROOF OF EQ. (30)

From $2\theta_1 = 2\alpha - \arcsin(-\tan 2\chi)$, Eq. (24), we have

$$\sin(2\alpha - 2\theta_1) = -\tan 2\chi, \tag{A1}$$

and from $2\theta_2 = 2\alpha + \arcsin(-\tan 2\chi) - \pi$, Eq. (25), we have

$$\sin(2\alpha - 2\theta_2) = -\tan 2\chi. \tag{A2}$$

Thus, replacing θ_1 or θ_2 in Eq. (18), we obtain

$$\mathbf{S}'_{\text{cross}} = \begin{pmatrix} 1 \\ \cos 2\chi \cos 2\alpha \\ \cos 2\chi \sin 2\alpha \\ -\sin 2\chi \end{pmatrix}, \tag{A3}$$

which corresponds to Eq. (28), obtained in Section 4.

APPENDIX B: PROOF OF EQS. (30) AND (31)

Defining $2\theta_\pm = 2\alpha \pm \pi/2$ replacing in Eq. (18), we have

$$\begin{aligned}\mathbf{S}'_\pm = (&1, \cos 2\chi \cos 2\alpha + [\cos 2\chi \sin(2\alpha - 2\alpha \mp \pi/2) \\ &+ \sin 2\chi] \sin(2\alpha \pm \pi/2), \\ &\cos 2\chi \sin 2\alpha - [\cos 2\chi \sin(2\alpha - 2\alpha \mp \pi/2) \\ &+ \sin 2\chi] \cos(2\alpha \pm \pi/2), \\ &\cos 2\chi \sin(2\alpha - 2\alpha \mp \pi/2)),\end{aligned} \tag{B1}$$

simplifying

$$\begin{aligned}\mathbf{S}'_\pm = (&1, \cos 2\chi \cos 2\alpha - (\cos 2\chi \mp \sin 2\chi) \cos 2\alpha, \\ &\cos 2\chi \sin 2\alpha - (\cos 2\chi \mp \sin 2\chi) \sin 2\alpha, \\ &\mp \cos 2\chi).\end{aligned} \tag{B2}$$

We finally obtain

$$\mathbf{S}'_\pm = \begin{pmatrix} 1 \\ \pm \sin 2\chi \cos 2\alpha \\ \pm \sin 2\chi \sin 2\alpha \\ \mp \cos 2\chi \end{pmatrix}, \tag{B3}$$

So, $\mathbf{S}_{\text{lower}} = \mathbf{S}_-$ [Eq. (29)] and $\mathbf{S}_{\text{upper}} = \mathbf{S}_+$ [Eq. (30)].

Funding. Universidad Industrial de Santander-Colombia; Departamento Administrativo de Ciencia, Tecnología e Innovación (Colciencias).

Acknowledgment. This work has been partially supported by the Vicerrectoría de Investigación y Extensión of the Universidad Industrial de Santander–Colombia. K. Salazar-Ariza acknowledges the financial support of Colciencias. The authors are grateful to Prof. P. Pellat-Finet for his valuable assistance.

REFERENCES

1. D. H. Goldstein, *Polarized Light* (CRC Press, 2016).
2. H. Fujiwara, *Spectroscopic Ellipsometry: Principles and Applications* (Wiley, 2007).
3. W. Shurcliff, *Polarized Light: Production and Use* (Harvard University, 2013).
4. A. Roberts and L. Lin, "Plasmonic quarter-wave plate," Opt. Lett. **37**, 1820–1822 (2012).
5. N. Yu, F. Aieta, P. Genevet, M. A. Kats, Z. Gaburro, and F. Capasso, "A broadband, background-free quarter-wave plate based on plasmonic metasurfaces," Nano Lett. **12**, 6328–6333 (2012).
6. R. Azzam, "Stokes-vector and Mueller-matrix polarimetry," J. Opt. Soc. Am. A **33**, 1396–1408 (2016).
7. D. H. Goldstein, "Mueller matrix dual-rotating retarder polarimeter," Appl. Opt. **31**, 6676–6683 (1992).
8. W. S. Bickel, J. Davidson, D. Huffman, and R. Kilkson, "Application of polarization effects in light scattering: a new biophysical tool," Proc. Natl. Acad. Sci. USA **73**, 486–490 (1976).

9. T. Yasui, Y. Tohno, and T. Araki, "Determination of collagen fiber orientation in human tissue by use of polarization measurement of molecular second-harmonic-generation light," Appl. Opt. **43**, 2861–2867 (2004).
10. V. Sankaran, J. T. Walsh, and D. J. Maitland, "Comparative study of polarized light propagation in biologic tissues," J. Biomed. Opt. **7**, 300–306 (2002).
11. M. Everett, K. Schoenenberger, B. Colston, and L. Da Silva, "Birefringence characterization of biological tissue by use of optical coherence tomography," Opt. Lett. **23**, 228–230 (1998).
12. J. Ladd, A. D. Taylor, M. Piliarik, J. Homola, and S. Jiang, "Label-free detection of cancer biomarker candidates using surface plasmon resonance imaging," Anal. Bioanal. Chem. **393**, 1157–1163 (2009).
13. C. Browne and F. Zerban, *Physical and Chemical Methods of Sugar Analysis: A Practical and Descriptive Treatise for Use in Research, Technical, and Control Laboratories* (Wiley, 1941).
14. P. A. Williams, "Rotating-wave-plate Stokes polarimeter for differential group delay measurements of polarization-mode dispersion," Appl. Opt. **38**, 6508–6515 (1999).
15. J. De Feijter, D. J. Benjamins, and F. Veer, "Ellipsometry as a tool to study the adsorption behavior of synthetic and biopolymers at the air-water interface," Biopolymers **17**, 1759–1772 (1978).
16. F. Xu, C.-C. Cheng, A. Scherer, R.-C. Tyan, P.-C. Sun, and Y. Fainman, "Fabrication, modeling, and characterization of form-birefringent nanostructures," Opt. Lett. **20**, 2457–2459 (1995).
17. I. Richter, P.-C. Sun, F. Xu, and Y. Fainman, "Design considerations of form birefringent microstructures," Appl. Opt. **34**, 2421–2429 (1995).
18. T. Sato, T. Araki, Y. Sasaki, T. Tsuru, T. Tadokoro, and S. Kawakami, "Compact ellipsometer employing a static polarimeter module with arrayed polarizer and wave-plate elements," Appl. Opt. **46**, 4963–4967 (2007).
19. J. M. López-Téllez, N. C. Bruce, and O. G. Rodrguez-Herrera, "Characterization of optical polarization properties for liquid crystal-based retarders," Appl. Opt. **55**, 6025–6033 (2016).
20. S. G. Reddy, S. Prabhakar, P. Chithrabhanu, R. Singh, and R. Simon, "Polarization state transformation using two quarter wave plates: application to Mueller polarimetry," Appl. Opt. **55**, B14–B19 (2016).
21. R. M. A. Azzam, "Poincaré sphere representation of the fixed-polarizer rotating-retarder optical system," J. Opt. Soc. Am. A **17**, 2105–2107 (2000).
22. A. Ambirajan and D. C. Look, "Optimum angles for a polarimeter: part I," Opt. Eng. **34**, 1651 (1995).
23. A. Ambirajan and D. C. Look, "Optimum angles for a polarimeter: part II," Opt. Eng. **34**, 1656–1658 (1995).
24. J. S. Tyo, D. L. Goldstein, D. B. Chenault, and J. A. Shaw, "Review of passive imaging polarimetry for remote sensing applications," Appl. Opt. **45**, 5453–5469 (2006).
25. D. Sabatke, M. Descour, E. Dereniak, W. Sweatt, S. Kemme, and G. Phipps, "Optimization of retardance for a complete Stokes polarimeter," Opt. Lett. **25**, 802–804 (2000).
26. R. M. A. Azzam and N. Bashara, *Ellipsometry and Polarized Light, North-Holland Personal Library* (North-Holland, 1987).
27. S. G. Reddy, S. Prabhakar, A. Aadhi, A. Kumar, M. Shah, R. Singh, and R. Simon, "Measuring the Mueller matrix of an arbitrary optical element with a universal SU(2) polarization gadget," J. Opt. Soc. Am. A **31**, 610–615 (2014).
28. G. Monge, *Géométrie descriptive: leçons données aux écoles normales, l'an 3 de la république* (Baudouin, imprimeur du Corps Legislatif et de l'Institut National, 1798).
29. R. Ferréol and J. Mandonnet, "Courbe de Viviani = Viviani's curve = Vivianische Kurve," in Encyclopédie des formes mathématiques remarquables, 2016, http://www.mathcurve.com/courbes3d/viviani/viviani.shtml.
30. J. Oprea, *Differential Geometry and Its Applications* (MAA, 2007).
31. E. Abbena, S. Salamon, and A. Gray, *Modern Differential Geometry of Curves and Surfaces with Mathematica*, 3rd ed., Textbooks in Mathematics (Taylor & Francis, 2006).
32. P. Baudoin, *Les ovales de Descartes et le limaçon de Pascal, Mathématiques elémentaires* (Vuibert, 1938).
33. J. Lawrence, *A Catalog of Special Plane Curves, Dover Books on Advanced Mathematics* (Dover, 1972).